Future Energy
Open Access Journal
ISSN 2832-0328

August 2024| Volume 03 | Issue 03 | Pages 33- 48

Journal homepage: https://fupubco.com/fuen

https://doi.org/10.55670/fpll.fuen.3.3.4

Future Publishing LLC

Article

Improved photovoltaic energy production under partial shading using an innovative MPPT controller based on Flying Squirrel Search Optimization algorithm

Diatta Sene[1]*, Adama Sarr[1], Mohamed Koïta Sako[2], Adama Ouattara[3], Mouhamadou Falilou Ndiaye[1], Vincent Sambou[1]

[1]Laboratoire Eau, Energie, Environnement et Procédés Industriels (LE3PI), Ecole Supérieure Polytechnique, Université Cheikh Anta Diop Dakar, Senegal
[2]Laboratoire Mécanique et Sciences des Materiaux, Institut Nationale Polytechnique, Félix HOUPHOUËT-BOIGNY Yamoussokro, Cote d'Ivoire
[3]Laboratoire des procédés industriels, des synthèses et des énergies renouvelables Institut Nationale Polytechnique, Félix HOUPHOUËT-BOIGNY Yamoussokro, Cote d'Ivoire

ARTICLE INFO

Article history:
Received 13 March 2024
Received in revised form
15 April 2024
Accepted 23 April 2024

Keywords:
PV systems, MPPT, Optimization, PV power, Partial shading, algorithms

*Corresponding author
Email address:
diattasene3s@gmail.com

DOI: 10.55670/fpll.fuen.3.3.4

ABSTRACT

This paper explores the issue of partial shading (PS) in photovoltaic systems and proposes a solution using the Flying Squirrel Search Optimization (FSSO) algorithm. PS results in power losses, and our study aims to enhance photovoltaic energy production by introducing a new Maximum Power Point Tracking (MPPT) controller based on the FSSO algorithm. This paper presents a controller designed to efficiently track the maximum power in the presence of partial shading. The controller uses the Modified ODD-EVEN (MOE) configuration, the Modified Symmetrical Array (MSA), and the Total-Cross-Tied (TCT). The performance of the FSSO algorithm was compared with that of GWO and PSO. A bidirectional DC-DC converter was integrated to connect the PV system to a battery. The proposed methods were also applied to an electric vehicle powered by a PV battery. The FSSO proposed in this study demonstrates an efficiency of over 99%, outperforming other methods in tracking the maximum power point and converging faster to the overall maximum power point. The results indicate that convergence time can be improved from 16% to over 60%. Furthermore, the proposed MPPT technique effectively minimizes over 80% of random oscillations. The proposed method reduces losses and maximizes fill factor compared to alternative algorithms, based on two observed shading cases. When connecting the system to a battery, the FSSO algorithm outperforms the PSO by more than 34.78% and the GWO by 49.02%. Although slightly inferior to the PSO, the FSSO still performs significantly in the context of an electric vehicle powered by a photovoltaic battery.

1. Introduction

Partial shading is a significant concern that must be considered during the installation of a photovoltaic system. It can significantly reduce the power output of a PV array and disrupt its operation by forming several local points on the power-voltage (P-V) characteristic curve. According to N. RAKESH et al. [1] in their work, the 'magic square' method can be used to increase the power generated by configuring the modules of a shaded 4x4 matrix photovoltaic array. In their study, Pareek et al. [2] proposed the SP and TCT configurations using a 2x2 PV array to investigate the impact on the maximum power point. Tatabhatla et al. [3] introduced a new configuration technique called Arrow Sudoku for all conventional configurations. Etarhouni et al. [4] combined three techniques with a closed-loop control strategy by subdividing the modified Magic Square-Enhanced Configuration (MS-EC) into four 3x3 TCT sub-arrays using a 6x6 PV array. Compared to TCT and MS-EC, this method

shows an improvement ranging from 11% to 48%. Ajmal et al. [5] conducted a comparative study of existing reconfiguration approaches to determine the constraints of each method. According to Sugumar et al. [6], the conventional method is impractical due to regular load disconnection from the solar PV array. They propose a new technique capable of detecting partial shading in real-time. Rezazadeh et al. [7] compared their static prime number approach with TCT, Sudoku, optimal Sudoku, improved Sudoku, and dominance square methods. They concluded that their approach is more optimal. Zeeshan et al. [8] developed a row indexing technique that uses the indexes of the reconfiguration matrix based on the state of the network. This method outperforms methods such as Sudoku, TCT, Chess-Knight, and PSO. Djilali et al. [9] studied three new physical arrangements of PV panels to maximize the power output of a PV array. These arrangements included the physical location of the S-M-TCT arrangement, the electrical connection of the S-M-TCT arrangement, and the electrical connection of the parallel S-M-TCT arrangement. These three new arrangements give better performance compared with the TCT, SP and Su Do Ku arrangements. K. Faldu et al. [10] compared the symmetrical array (SA) configuration with the Bridge-Link (BL), Series-Parallel (SP), Total-Cross-Tied (TCT), and Honey-Comb (HC) configurations and found that the former performed better. Yadav et al. [11] studied the performance of 4x4 PV array configurations, including TCT, hybrids SP-TCT, BL-TCT, BL-HC, and rearranged configurations RTCT, RSP-TCT, RBL-TCT, RBL-HC based on a magic square (MS). In most cases where shading was present, the MS-based arrangements resulted in minimal power losses and a higher fill factor for the PV array. Dhanalakshmi et al. [12] compared four different shading models, including the existing TCT method, the 'dominance square' (DS) method recently proven in the literature, and their proposed 'competence square' (CS) method. The CS technique outperformed the other methods in terms of minimizing row current, achieving maximum power, and minimizing losses. Satpathy et al. [13] demonstrated that the output power of the array is dependent not only on the topology but also on the shading characteristics. Deshkar et al. [14] proposed a reconfiguration scheme based on genetic algorithms, which resulted in a uniform distribution of shadow over the module and prevented concentration on a single row. The proposed method outperforms both the TCT and Su Do Ku arrangement. Harrag et al. [15] suggested a reconfiguration algorithm that uses the genetic algorithm (GA) to automatically reconfigure the SP topology of a 4x4 PV array. The study's results demonstrated an efficiency improvement ranging from 6.49% (limited shading) to 71.03% (shading of large areas) in all cases studied. Mohammad et al. [16] work presents a new hybrid MPPT approach that uses a modified P&O method assisted by the Extremum Seeking Control (ESC) strategy. The proposed algorithm's performance is compared to that of conventional algorithms (P&O), confirming its effectiveness. Winston et al's [17] experimental study on the 3x3 Total Cross Tied (TCT) PV array connected by three converters demonstrated the cancellation of unbalance losses, resulting in improved performance compared to other configurations such as the offset-based configuration, Su Du Ko configuration, simple static configuration, and conventional TCT configuration. Pachauri et al.'s work [18] provides a literature review of models that can mitigate the effects of partial shading and ranks their performance for each subgroup. Kacimi et al. [19] developed a new approach by combining the Grasshopper Optimization Algorithm (GOA) and Model Predictive Controller (MPC) methods. This approach is more efficient and produces higher output power amplitude than the PSO, PSO-MPC, and GOA methods. The literature presents case studies where the squirrel search algorithm has been used for several global optimization problems [20-22]. In other cases, a hybrid algorithm of particle swarm optimization and flying squirrel search optimization has been employed [23]. The objective of this study is to achieve optimal production of solar PV energy. The presented method is based on the FSSO algorithm, which provides several advantages, including faster tracking of the maximum power point (MPP), reduced computational load, decreased energy production losses, and improved overall efficiency.

2. Modelling a photovoltaic (PV) cell under partial shading conditions

This section discusses the mathematical representation of a photovoltaic module using a dual diode model. Additionally, we detail the partial shading condition used to evaluate the effectiveness of the suggested methods. To implement the Maximum Power Point Tracking (MPPT) technique, a boost DC-DC converter is used as an interface between the photovoltaic modules and the load. This section also describes the operation of a conventional boost converter.

2.1 Double diode PV cell model

The single diode model is the most commonly used model to represent PV cells due to its simplicity and accuracy. However, more accurate models, such as the two-diode model in Figure 1, have been developed [24-26]. This model provides a more precise representation of PV cells.

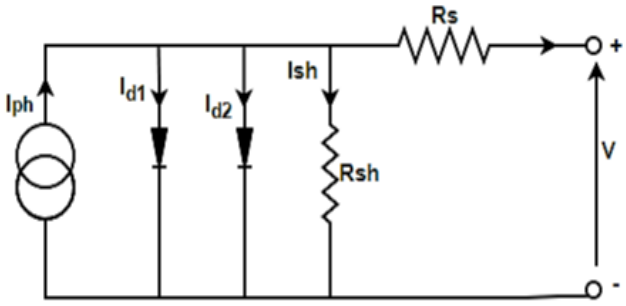

Figure 1. Two-diode model of a photovoltaic cell

The model comprises of two diodes, a current generator, and two resistors. Solving the equivalent circuit above results in the following implicit expression for the current I [27, 28].

$$I = I_{ph} - I_{d1}\left[Exp\left(\frac{V+IR_s}{V_{T1}}\right)-1\right] - I_{d2}\left[Exp\left(\frac{V+IR_s}{V_{T2}}\right)-1\right] - \frac{V+IR_s}{R_{sh}} \quad (1)$$

$$V_{T1,2} = \frac{n_{1,2}\times N_s KT}{q} \quad (2)$$

Where I_{ph} is the current produced by the incident light. $I_{d1,2}$ are the reverse saturation currents of diode 1 and diode 2 respectively. $V_{T1,2}$ is the thermal voltage of the PV module with N_s cells connected in series. q is the electron charge, k is Boltzmann's constant, T is the absolute temperature of the P-N junction in Kelvin K. The variables n_1 and n_2 represent the diffusion and recombination current, respectively, of the components of diodes 1 and 2. Finally, R_{sh} is the parallel resistance and R_s is the series resistance. To optimize their performance, photovoltaic systems must operate at their maximum power point. This point fluctuates according to environmental conditions such as temperature and irradiation levels. To increase the power generated, it is possible to connect several photovoltaic panels using different configurations, including TCT, MSA, and MOE. However, some solar panels may experience a drop in voltage and behave similarly to a load. This can be caused by irregularities in irradiation levels, such as partial shading, as shown in Figure 2. The phenomenon described is referred to as partial shading (PS), which results in a mismatch effect. The I-V (current-voltage) and P-V (power-voltage) curves indicate the point of maximum power under uniform irradiation conditions, as illustrated in Figure 3. It is crucial to note that mismatches create hot spots.

To mitigate these effects, it is recommended to use a bypass diode, which induces multiple peaks in the I-V and P-V curves, as shown in Figure 4. According to the work of [29], under partial shading conditions, the P-V curve shows several local maxima (LM), while there is only one global maximum (GM). Therefore, it is crucial for photovoltaic systems to always operate at the global maximum to optimize the extraction of available solar energy.

2.2 Boost converter

To optimize the efficiency of a photovoltaic (PV) panel and transfer the maximum power to the load, a boost DC-DC converter is used as the link between the PV panel and the load, as shown in Figures 5, according to [30]. To implement maximum power point tracking (MPPT), the duty cycle is regulated by the MPPT controller. The MPPT controller generates a control signal that varies in the range of [0, 1] [31]. The DC boost converter has several essential parameters, including switching frequency (F), output voltage (V_{out}), input voltage (V_{in}), output capacitance (C_{out}), input capacitance (C_{in}), inductance value (L), load ripple current (ΔI_{load}), load ripple voltage (ΔV_{load}, equivalent to 2% de V_{out}), input ripple voltage (ΔV_{load}, corresponding to 1% de V_{in}) and duty cycle (D).

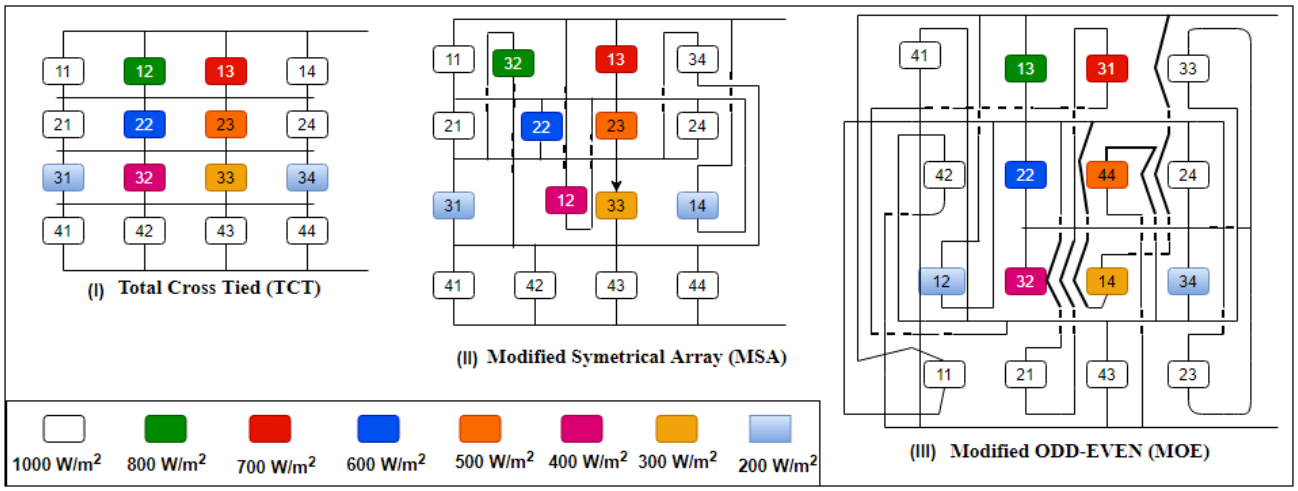

Figure 2. Solar module connected under uniform and non-uniform irradiation

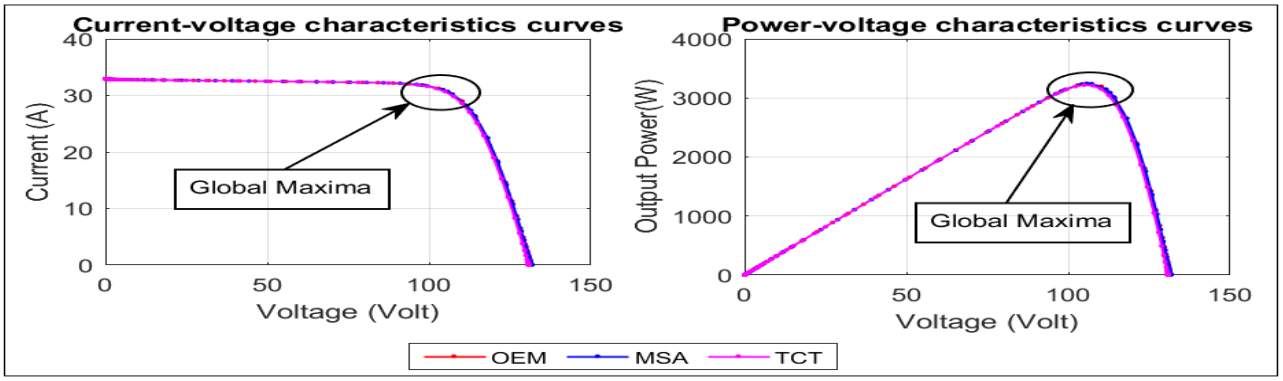

Figure 3. I–V and P–V curves under uniform irradiance

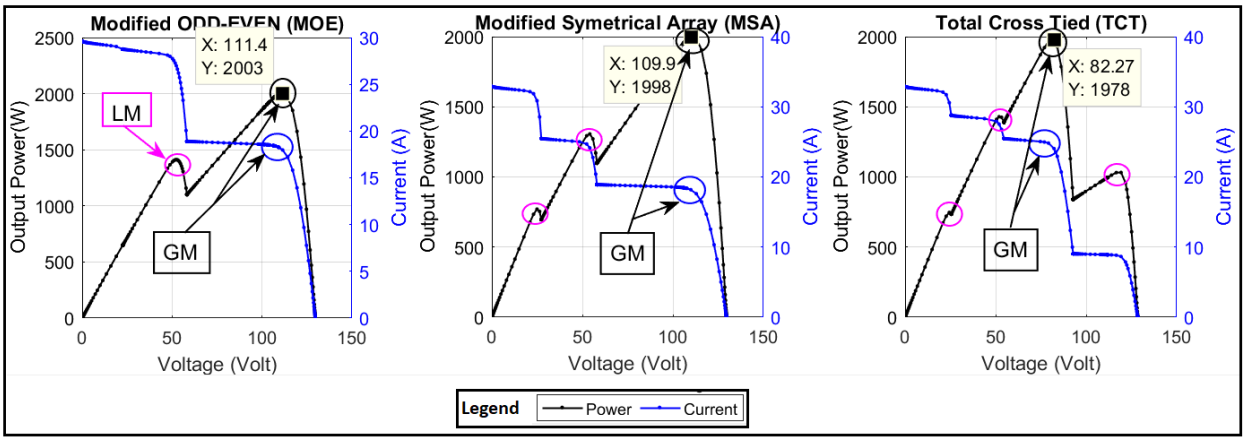

Figure 4. I–V and P–V curves under partial shading condition

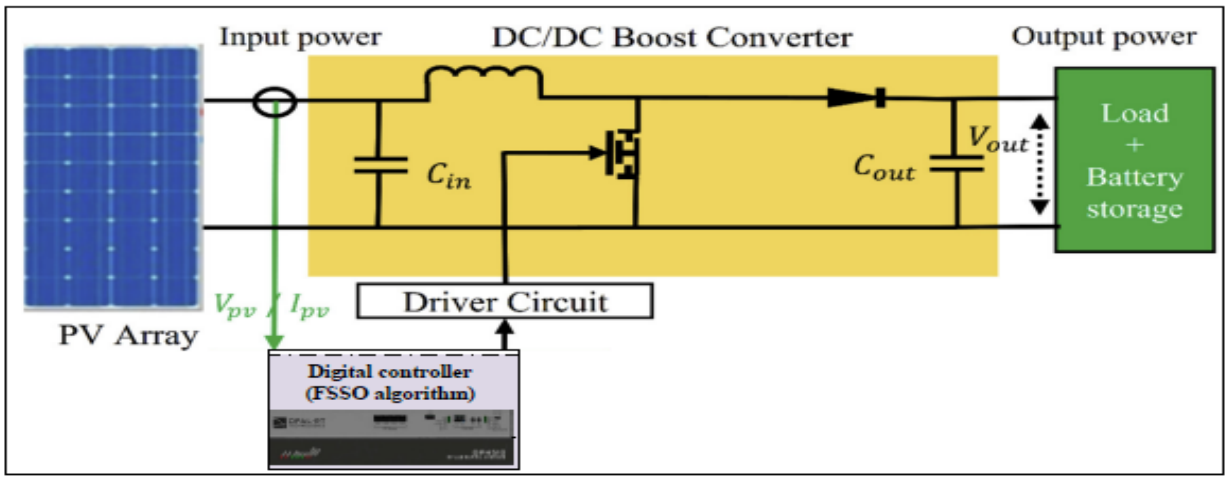

Figure 5. Schematic of the planned Photovoltaic Test System

Equations (1) to (5) provide the corresponding mathematical model.

$$V_{out} = \frac{V_{in}}{1-D} \quad (1)$$

$$D = \frac{t_{on}}{t_{switching}} \quad (2)$$

$$L = \frac{D\times(1-D)^2\times R_L}{2\times F} \quad (3)$$

$$C_{in} = \frac{D}{8\times F^2\times L\times 0.01} \quad (4)$$

$$C_{out} = \frac{D}{0.02\times F\times R_L} \quad (5)$$

3. Methodologies

3.1 PV panel configurations

In the literature, various researchers [32, 33] have developed several configurations of PV module to optimize the production of solar power plants.

Total Cross Tied (TCT) :

TCT involves connecting all the solar modules in parallel on the same line in different strings. This creates a solar field that resembles a matrix with several nodes.

The sum of the currents in the different nodes and the voltage of the solar modules connected in parallel are equal. The current produced by the 4x4 modules in the PV array depends on the irradiance G and can be calculated using the following formula [34]:

$$I = \frac{G}{G_0} \times I_m \quad (6)$$

Where I_m is the current generated by the module for irradiation under Standard Test Conditions (STC) of 1000W/m² and a temperature of 25°C. The PV array voltage can be calculated as follows [35]:

$$V_{array} = \sum_{i=1}^{4} V_i \quad (7)$$

Where V_{array} is the PV array voltage and V_i is the maximum array voltage of the panels in the nth row. The calculation of current limit for any array, depending on the configuration, can be calculated as follows [36]:

$$I_{Rn} = \sum_{n=1}^{n} I \quad (8)$$

Modified Symetrical Array (MSA) and Modified ODD-EVEN configuration:

The Modified Symmetrical Array (SA) and Modified ODD-EVEN (MOE) are puzzle-based configurations. Figure 2 (II) and 2 (III) show the schematics of these configurations.

3.2 Description of flying squirrel search optimization

The FSSO algorithm replicates the dynamic method used by Flying Squirrels (FS) when searching for food. The position of an FS represents the potential solution vector, while the quality of the food corresponds to the amplitude of the vector. The amplitude values were initially divided into three zones: the optimal solution (OS), the quasi-optimal solution (QOS), and the random solution (RS). For Maximum Power Point Tracking (MPPT), the target (food source) is the power of the PV panel. The decision variable (position) is specified by the utilization rate D of the inverter. The FSSO algorithm aims to eliminate the looter to minimize the time taken to reach the global maximum power point (GMPP) [37]. The flowchart in Figure 6 shows the various stages of the FSSO algorithm, along with equations 9 to 19 [38, 39].

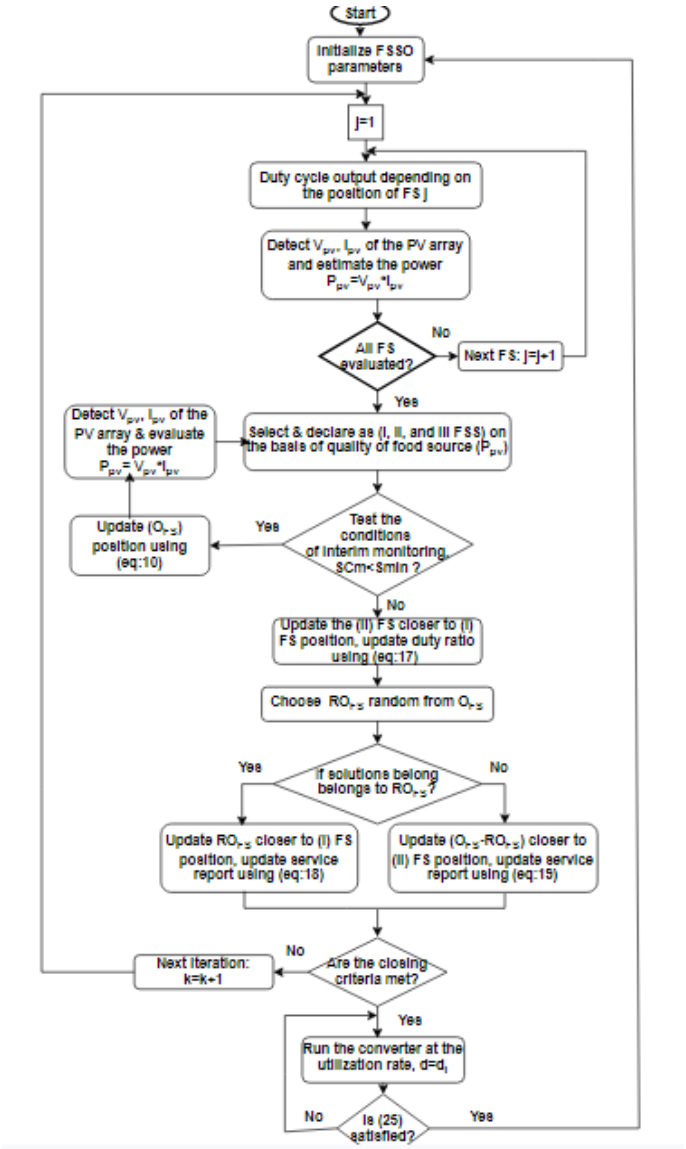

Figure 6. Flowchart of the algorithm of the proposed FSSO method

a. Initialisation

Assuming N_{FS} represents the population size and dU and dL represent the upper and lower limits of the duty cycle for boost mode operation, respectively, with stabilization of 0.75 and 0.3 of the proper duty cycle. F_{Sj} individuals are randomly generated using equation 9.

$$FS_j = d_L + \frac{[d_U - d_L](j-1)}{N_{FS}} \; ; j = 1,2 \ldots ; N_{FS} \tag{9}$$

Note that the limiting constraints are such that :

$$0 < FS_j < 0.5 \tag{10}$$

b. Estimating physical condition

At this level, the converter's work with each FS position is recorded. The instantaneous power P_{pv}(FS) is estimated as the objective (food source) for each FS duty ratio. The objective function (F) for maximum power point tracking is expressed and repeated for all duty ratios.

$$F(FS) = maxP_{pv}(FS) \tag{11}$$

c. Reporting and selection

In this phase, the service rate is reported alongside the PV power at position (I). The next most optimal FS position is in position (II), while the other FS (O_{FS}) is located at position (III).

d. Updating positions

Before updating the duty cycle action, it is necessary to test the provisional control capability. To do so, the duty cycles can only be updated using method (i) if the following conditions are met: $\boldsymbol{S_C^k < S_{min}}$. After this step, competence can be estimated. Otherwise, the service cycles are updated using method (ii).

Method (i): Provisional control condition

Including a control condition prevents the algorithm from being affected by the local maximum power point. Equation 12 provides the expression for the one-dimensional space of the provisional constant (S_C^k) and the minimum value (S_{min}) [40].

$$\begin{cases} S_C^k = \sqrt{\sum_{k_1}^{F_d} \left(|d_{II}^k - d_I|\right)^2} \\ S_{min} = \frac{10exp(-6)}{365^{k/(k_m/2.5)}} \end{cases} \tag{12}$$

d_{II}^k : FS position at position (II) ;
d_I : Position of the FS at position (I) ;
k : Number of iterations and $k_m$the maximum number of iterations.

The Levy distribution is used to locate the other FS at position (III) in order to improve prospecting.

$$d_{III}^{k+1} = d_{III}^k + S_l \tag{13}$$

d_{III} is the position of the FS on (III) and S_L the step length and is expressed at least in terms of the Levy distribution.

$$S_L \approx k_c \left(\frac{u}{|v|^{\frac{1}{\beta}}}\right)(d_I - d_{III}) \tag{14}$$

β : Levy index, its value is 1.5 ;
k_c : Step coefficient, its value is 1.5 ;
u and v determined by the normal distribution curve;

$$u \approx n(0, \sigma_u^2) \quad (15)$$

$$v \approx n(0, \sigma_v^2) \quad (16)$$

The expression of σ_u is given by equation (17), where Γ is the integral function:

$$\sigma_u = \left(\frac{\Gamma \times (1+\beta) \times \sin\left(\frac{\pi\beta}{2}\right)}{\Gamma \times \left(\frac{1+\beta}{2}\right) \times \beta \times 2^{\left(\frac{\beta-1}{2}\right)}} \right)^{\frac{1}{\beta}} \quad (17)$$

The expression of σ_v is given by equation (18), and Γ is the integral function is given by equation (19):

$$\sigma_v = 2 \quad (18)$$

$$\Gamma(n) = (n-1)! \quad (19)$$

Method (ii): Regular updating

The positions of the FS are updated by moving to positions (I), (II), or (III) in the order given by equations (20) to (22) [41,42].

$$d_{II}^{k+1} = d_{II}^{k} + d_g G_c \left(d_I^k - d_{II}^k\right) \quad (20)$$

$$d_{III}^{k+1} = d_{III}^{k} + d_g G_c \left(d_I^k - d_{III}^k\right) \quad (21)$$

$$d_{III}^{k+1} = d_{III}^{k} + d_g G_c \left(d_{II}^k - d_{III}^k\right) \quad (22)$$

G_c: Slip constant, set at a value equal to 0.0019.
d_g: Slip distance, expressed by equation (23).

$$d_g = \frac{h_g}{S_f \times tan\Phi} \quad (23)$$

$$tan\Phi = \frac{F_D}{F_L} \quad (24)$$

h_g: Value of the loss of height following glide, equal to 0.01 m.
S_f : Scale factor, its value is 0.18.
F_D : Drag force, its expression is given by equation (25).

$$F_D = \frac{1}{2}\rho V^2 S c_d \quad (25)$$

F_L: Lift force, equation (26) determines its expression.

$$F_L = \frac{1}{2}\rho V^2 S C_L \quad (26)$$

ρ : Air density; its value is 1.204 Kg/m³ ;
V : FS speed, its value is 0.0525 hm/s;
S : Surface area of the FS body, its value is 0.00154m² ;
c_d and C_L are the drag and lift coefficients, respectively.
The value of c_d is 0.006, while the value of C_L is 0.007.

e. Finding the common point

The algorithm suspends when the change in position of all the FS is below the initial point or when it reaches the maximum value of iterations, and the common point is obtained. The iterative ratio over which the converter's work follows the global maximum power point is acquired. Then, the FS positions are rebooted to find the new global maximum power point. The constraint equation for detecting the change in insolation is provided.

$$\frac{P_{pv}^{k+1} - P_{pv}^{k}}{P_{pv}^{k+1}} \geq \Delta P(\%) \quad (27)$$

3.3 Characteristics of the electrical properties of the PV panel and inverter

The characteristics of the PV panel used are shown in Table 1.

Table 1. PV module parameters (Kyocera Solar KC200GT)

Parameters	Values at STC	unit
Electrical properties		
Open circuit voltage (V)	32.9	(V)
Short circuit current (I)	8.21	(A)
Power at MPP (P)	200.143	(W)
Current at MPP (I)	7.61	(A)
Voltage at MPP (V)	26.3	(V)
Shunt resistance (R)	150.6921	(Ω)
Series resistance (R)	0.34483	(Ω)
Number of cells in series	54	
Temperature coefficients		
Temperature coefficient of V_{OC}	-0.35502	(%/deg.C)
Temperature coefficient of I_{SC}	0.06	(%/deg.C)

3.4 Presentation of the test installation for PV solar panels not connected to a battery

The impact of the FSSO algorithm on the energy production of the PV system was tested and compared to the performance of other algorithms such as Particle Swarm Optimisation (PSO) and Grey Wolf Optimisation (GWO). The Modified ODD-Even (MOE), Modified Symmetrical Array (MSA) and Total-Cross-Tied (TCT) configurations were tested in a 4x4 network. Figure 7 displays the simulation test diagram.

A comprehensive performance evaluation will be conducted to assess and contrast the efficacy of various approaches. Specifically, MOE_FSSO, MOE_GWO, MOE_PSO on one side, and MSA_FSSO, MSA_GWO, MSA_PSO on the other, along with TCT_FSSO, TCT_GWO, TCT_PSO will be evaluated. The evaluation will consider the maximum power point (P_M), the percentage of power losses due to mismatch (P_L) given by the equation (28) and the fill factor (F_f) expressed in equation (29) [43].

$$P_L = \frac{P_{M(STC)} - P_{M(PSC)}}{P_{M(STC)}} \quad (28)$$

$$F_f = \frac{I_{M(PSC)} V_{M(PSC)}}{I_{SC} V_{OC}} \quad (29)$$

$P_{M(STC)}$: Maximum power point under standard temperature conditions.
$P_{M(PSC)}$: Maximum power point under partial shading conditions.
$I_{M(PSC)}$: Maximum operating current under partial shading conditions.
$V_{M(PSC)}$: Maximum operating voltage under partial shading conditions.
I_{SC}: Short-circuit current.
V_{OC}: Open circuit voltage.
The fill factor ($\boldsymbol{F_f}$) is a crucial parameter that determines the power conversion efficiency of an organic solar cell [44]. The gains in the fill factor partly compensate for the losses due to the current mismatch [45]. It is a generic diagnostic indicator sensitive to power losses due to shading and faulty conditions occurring in PV systems. This parameter is sufficiently robust for changes in irradiance and temperature levels [46].

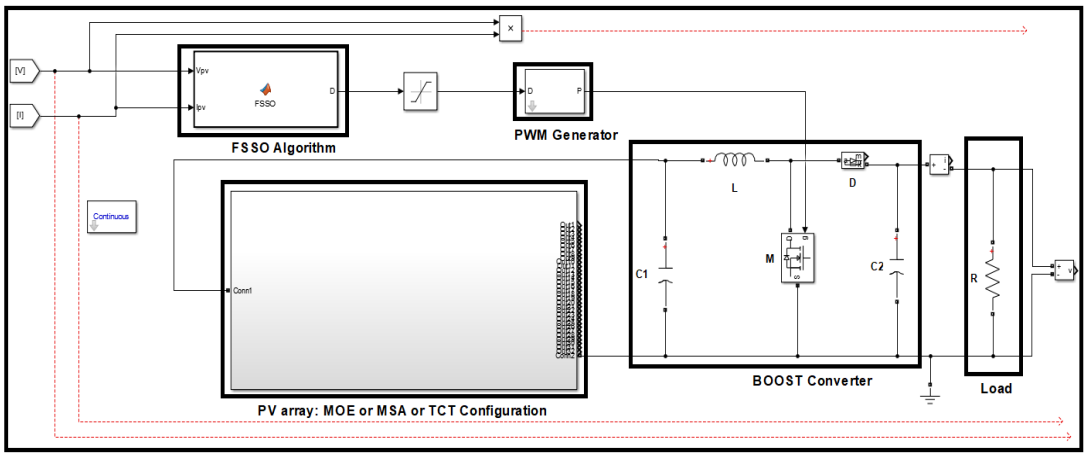

Figure 7. Schematic of the proposed PV solar array test setup

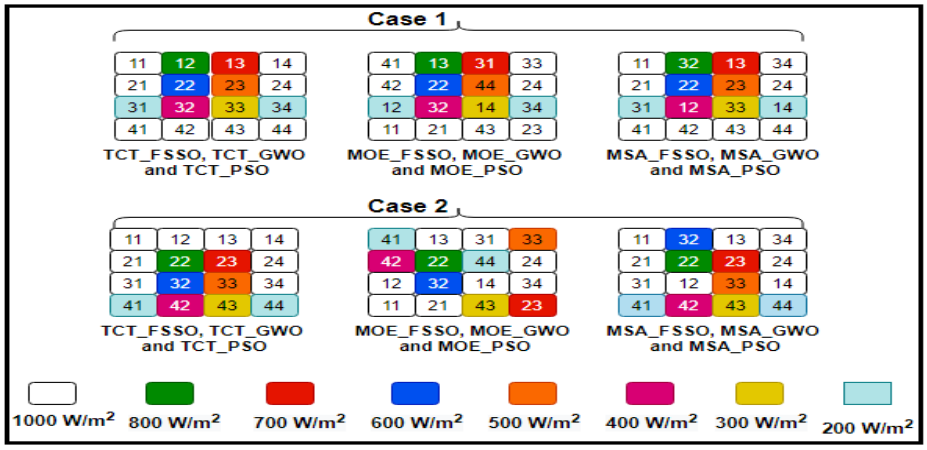

Figure 8. Diagram of the first and second cases of the shading pattern tested

4. Results and discussion

4.1 Optimization of power output and maximum power point tracking for a solar PV system

To enhance the power output of a photovoltaic array under partial shading conditions, we examined three configurations: Total Cross Tied (TCT), Modified Odd-Even (MOE), and Modified Symmetrical Array (MSA). Each configuration was integrated into a 4x4 matrix and partially regulated using the FSSO, GWO, or PSO algorithms. Figure 8 depicts the shading model employed. Figure 9 and Figure 10 display the results obtained from the FSSO, PSO, and GWO algorithms. The tests analyzed the power production behavior and performance under partial shading. Figures 9 and 10 demonstrate that when using the FSSO, GWO, or PSO algorithms to optimize maximum power point tracking (MPPT) in the three case configurations, the FSSO algorithm outperforms the GWO and PSO algorithms in terms of settling time, maximum power point (MPP), and efficiency. It was observed that the GWO algorithm exhibits continuous oscillations regardless of the configuration, resulting in less efficient stabilization and minimization of the maximum power point (MPP). In contrast, the FSSO and PSO algorithms exhibit less pronounced fluctuations than the GWO algorithm.

The FSSO algorithm stands out for its faster stabilization than the PSO algorithm, highlighting its efficiency and ability to maximize power output when tracking the maximum power point (MPPT). For a more detailed presentation of these results, please refer to Table 2 for the first case and Table 3 for the second case shading pattern.

Table 2 shows that in the MOE configuration, the FSSO algorithm achieves an efficiency of 99.98%, outperforming the GWO algorithm (99.96%) and the PSO algorithm (99.47%). Additionally, the FSSO algorithm demonstrates a remarkable ability to reduce stabilization time by 74% compared to GWO and by 50.91% compared to PSO. For the MSA configuration, the FSSO algorithm maintains its advantage with an efficiency of 99.96%, outperforming GWO (99.23%) and PSO (99.94%). In this configuration, FSSO reduces the stabilization time significantly, achieving a reduction of 73.33% compared to GWO and 45.32% compared to PSO. Finally, in the TCT configuration, the FSSO algorithm achieves an efficiency of 99.99%, outperforming GWO (99.97%) and PSO (99.96%). FSSO also achieves a significant reduction of 80.33% in stabilization time compared to GWO and 4.83% compared to PSO.

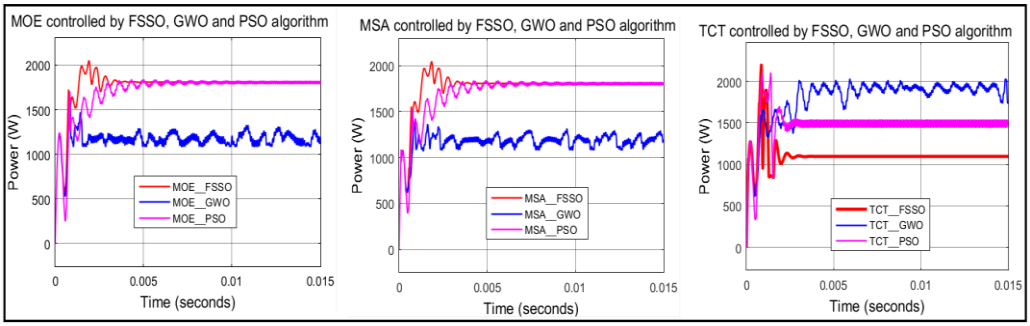

Figure 9. MPPT simulation results for the first case of partial shading

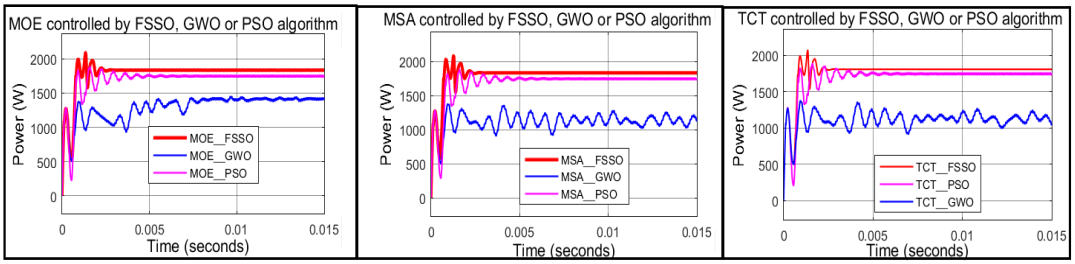

Figure 10. MPPT simulation results for the second case of partial shading

Table 2. Qualitative comparison of the FSSO algorithm with the GWO and PSO algorithms first case

Configuration	Technique	Converge Time (s)	Settling Time (s)	Power at GM (W)	Max Power (W)	Efficiency (%)
MOE	FSSO	0.001914	0.0039	2048	2047.60	99.98
MSA	FSSO	0.00185	0.004	2046	2045.27	99.96
TCT	FSSO	0.0008553	0.00295	2198	2197.87	99.99
MOE	GWO	0.0008408	LM	1603	1602.50	99.96
MSA	GWO	0.0009	LM	1386	1375.44	99.23
TCT	GWO	0.00592	LM	2029	2028.39	99.97
MOE	PSO	0.004313	0.007946	1839	1829.256	99.47
MSA	PSO	0.004915	0.007316	1840	1838.98	99.94
TCT	PSO	0.0014	0.00310	2106	2105.33	99.96

Table 3 presents results showing that the FSSO algorithm is more efficient than both the GWO algorithm and the PSO algorithm under the MOE configuration, with an efficiency rate of 99.96%. It is worth noting that the FSSO algorithm significantly reduces stabilization time by 70% compared to GWO and 53.75% compared to PSO. Under the MSA configuration, the FSSO algorithm maintains its advantage with an efficiency of 99.99%, outperforming GWO (99.97%) and PSO (99.35%). Additionally, FSSO significantly reduces the stabilization time, achieving an 81.66% reduction compared to GWO and a 56.45% reduction compared to PSO. In the TCT configuration, the FSSO algorithm achieves an efficiency of 99.95%, outperforming GWO (99.93%) and PSO (99.94%). In terms of stabilization time, FSSO achieves a significant reduction of 80.56% compared to GWO and 53.30% compared to PSO. Figure 11 visually represents these results, displaying the duty cycle of each algorithm throughout the optimization process.

The duty cycle curves for the FSSO algorithm show exceptional speed and efficiency in the search for optimal solutions, with almost no dips. This indicates a strong convergence towards an optimal or near-optimal solution. In contrast, the duty cycle curves of the FSSO algorithm remain relatively stable throughout its uptime, indicating that it spends less time exploring new regions and more time improving solutions. This highlights the superior performance of the FSSO algorithm compared to the GWO and PSO algorithms, which show dips in their duty cycle curves, suggesting limitations and delays. Figure 12 and Figure 13 demonstrate a complete evaluation of voltage and current transients for the two observed cases of partial shading.

Examining Figures 12 and 13, these diagrams demonstrate the significant surges resulting from the initial exploration of the search space. As the iterative time increases, the transients gradually progress towards greater stability, with the FSSO algorithm achieving this more rapidly. The aim is to achieve zero oscillations when the maximum power point (MPP) is reached. However, both the PSO and GWO methods still exhibit persistent random fluctuations, with the GWO algorithm showing them more frequently. In summary, the FSSO algorithm results in reduced oscillations in Maximum Power Point Tracking (MPPT) techniques compared to the GWO and PSO approaches. The proposed method consistently produces stable results, outperforming competing techniques such as GWO and PSO. It is important to note that there is minimal energy loss when the output remains stable. Figures 12 and 13 illustrate the boost converter in more detail using the voltage and current curves obtained during simulation of the PV system. The study demonstrates the impact of the FSSO algorithm on the output power of the boost converter. The results show a significant increase in the voltage supplied by the PV system compared to the GWO and PSO algorithms, regardless of the

configuration considered. Although the PSO algorithm also leads to a significant voltage increase, the intense oscillations of the output power accentuate the power losses, resulting in a lower voltage than the FSSO algorithm. To evaluate the effectiveness of the configuration methods used in this study, we analyzed the losses associated with each configuration type and evaluated the fill factor. The results are shown in Figure 14 and Figure 15.

Table 3. Qualitative comparison of the FSSO algorithm with the GWO and PSO algorithms first case

Configuration	Technique	Converge Time (s)	Settling Time (s)	Power at GM (W)	Max Power (W)	Efficiency (%)
MOE	FSSO	0.00135	0.00275	2094	2093.16	99.96
MSA	FSSO	0.001267	0.0027	2088	2087.928	99.99
TCT	FSSO	0.00135	0.002915	2074	2072.7836	99.94
MOE	GWO	0.009711	0.009418	1432	1379.4007	95
MSA	GWO	0.000942	LM	1378	1377.64	99.97
TCT	GWO	0.0009424	LM	1376	1375.40	99.93
MOE	PSO	0.001612	0.005947	1887	1886.01	99.94
MSA	PSO	0.001613	0.006316	1886	1836.1832	97.35
TCT	PSO	0.001615	0.006243	1889	1875.4999	99.94

Figure 14 shows the results of the initial partial shading scenario. The findings indicate that, regardless of the configuration used with optimization techniques, the FSSO algorithm consistently results in lower losses compared to alternatives such as GWO and PSO. Notably, the fill factor, a key determinant of system productivity, improves significantly when using the FSSO algorithm. The results demonstrate that the FSSO algorithm outperforms GWO and PSO in optimizing energy production of photovoltaic systems under partial shading conditions. It is important to note that, in this specific shading scenario, a comparative analysis of identical configurations using the same algorithm, specifically the TCT configuration, resulted in significant performance improvements. Figure 15 shows the recorded losses during the observation of the second partial shading scenario. The figure provides an interpretation of the fill factor generated by this specific shading scenario. Regarding the second case involving partial shading, Figure 15 displays the outcomes. The results consistently show that, regardless of the configuration used alongside optimization techniques, the FSSO algorithm outperforms other solutions such as GWO and PSO in minimizing losses.

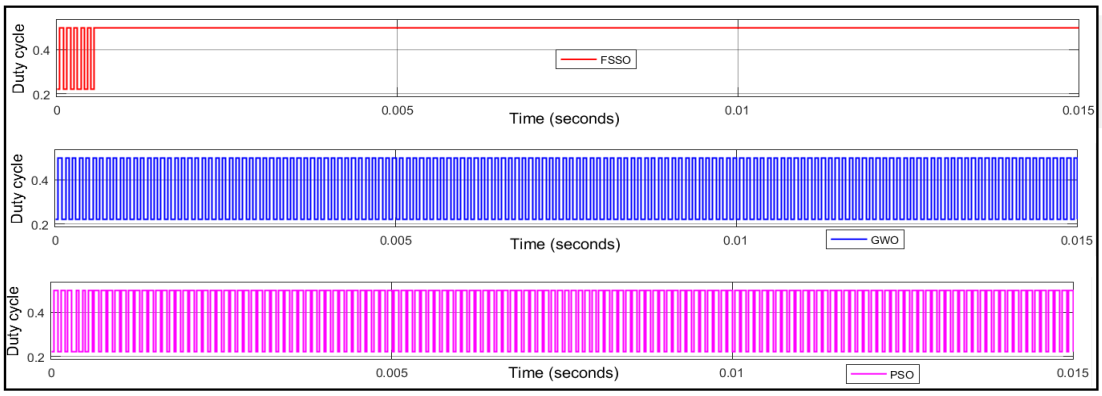

Figure 11. Duty cycle comparison of FSSO, GWO and PSO

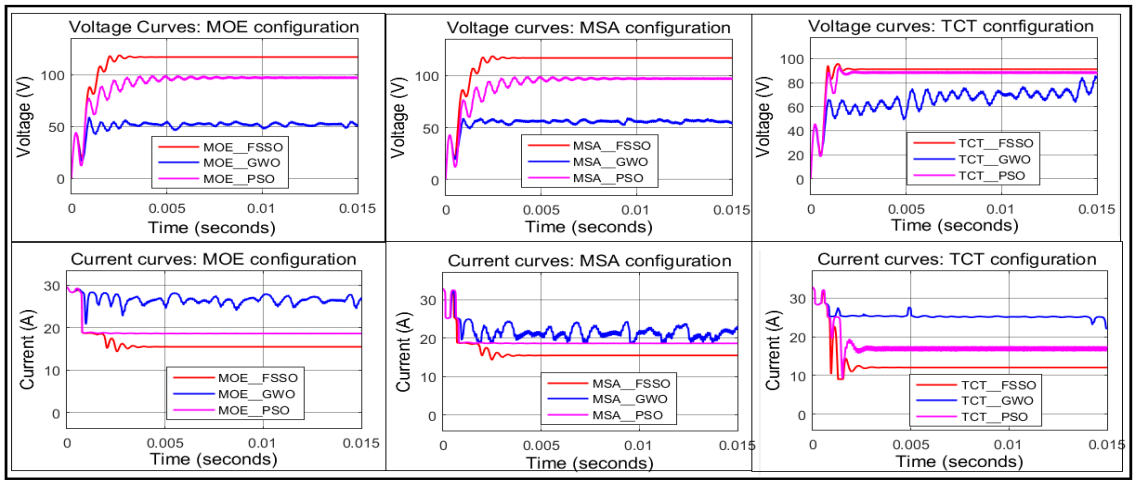

Figure 12. Results of the simulation of the voltage and current curves for the first case

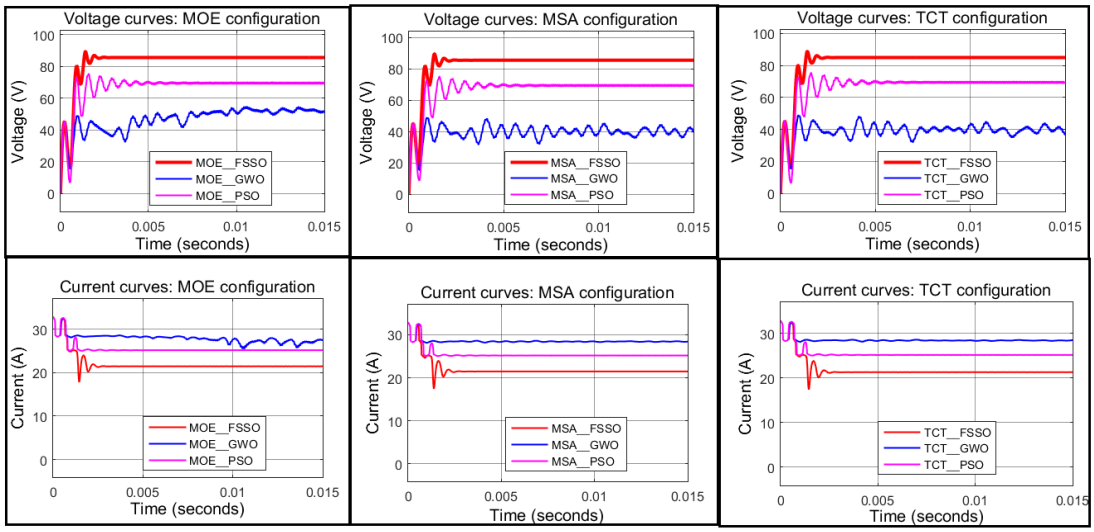

Figure 13. Results of the simulation of the voltage and current curves for the second case

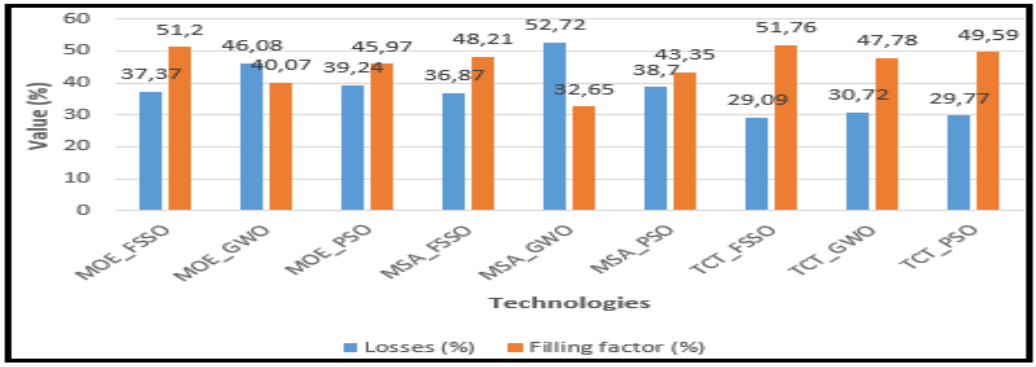

Figure 14. Representation of losses and fill factor first case

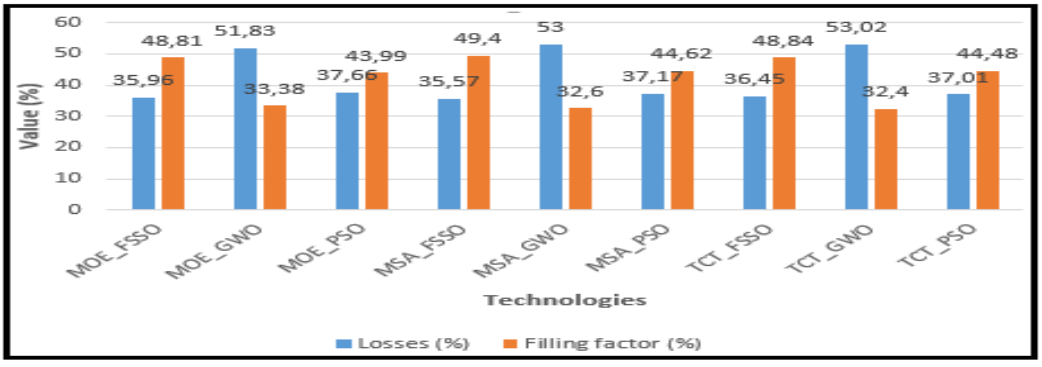

Figure 15. Representation of losses and fill factor second case

This highlights the continued importance of the FSSO algorithm compared to alternative approaches like GWO and PSO. The implementation of the FSSO algorithm notably enhances the fill factor. Based on these observations, we can assert that the FSSO algorithm is a superior solution for efficiently optimizing the energy production of photovoltaic systems under partial shading conditions.

4.2 Solar PV system connected to a battery

In this context, we propose a network configuration of 4 x 1. Table 4 presents the irradiation model. This sequence presents an examination of a photovoltaic (PV) system connected to a storage battery controlled by either the FSSO algorithm, the GWO algorithm, or the PSO algorithm. The results of these configurations are displayed in Figures 16-20.

Table 4. The irradiation pattern of the case observed

	Irradiance (W/m²)			
	PV_1	PV_2	PV_3	PV_4
Fast-moving cases	1000 ; 500 ; 750 ; 900	1000 ; 500 ; 750 ; 900	1000 ; 500 ; 750 ; 900	1000 ; 500 ; 750 ; 900

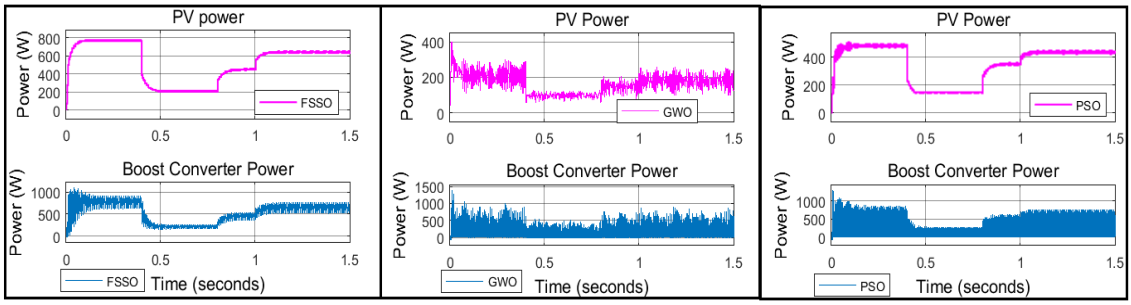

Figure 16. PV system and boost converter output results

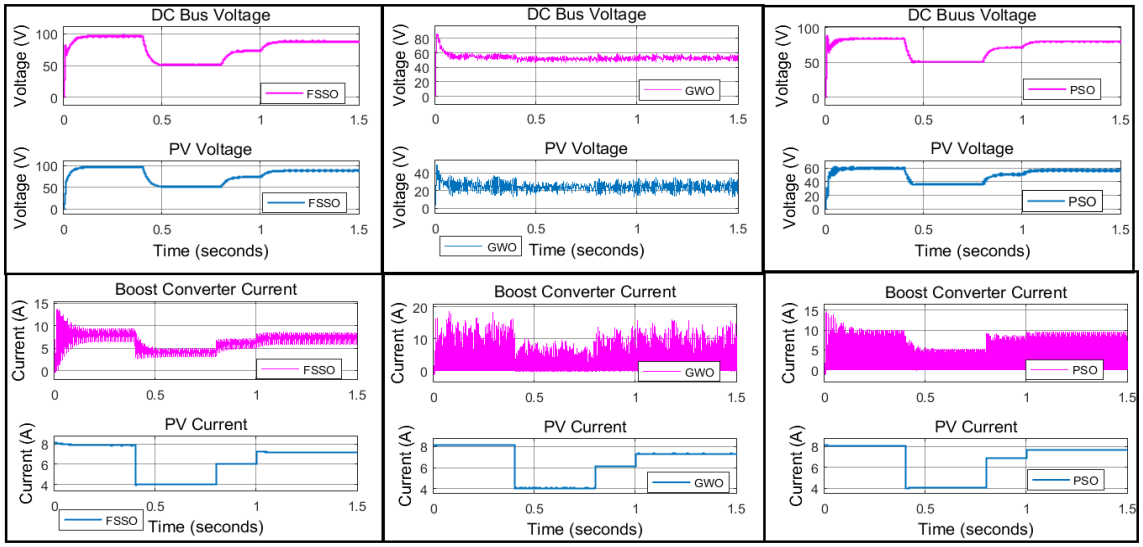

Figure 17. Voltage and current results

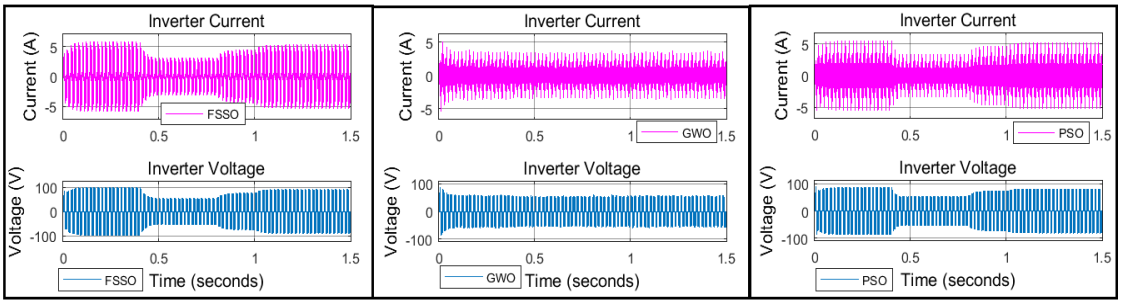

Figure 18. Inverter voltage and current results

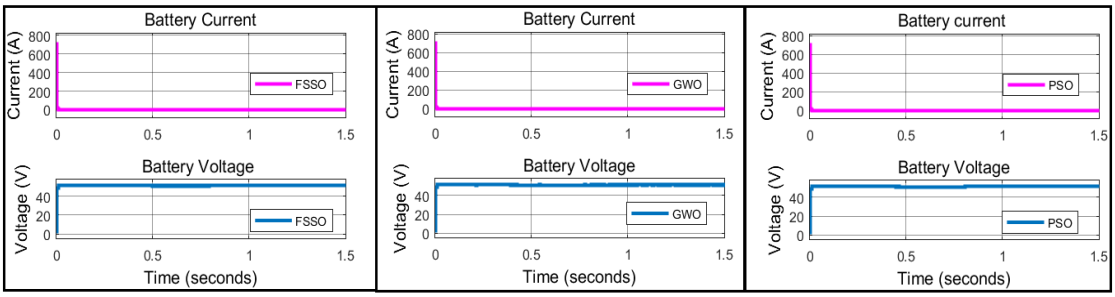

Figure 19. Storage battery current and voltage result

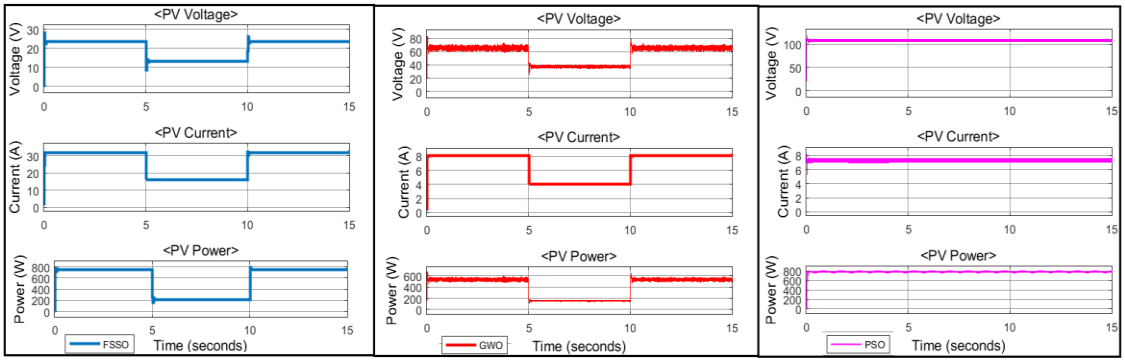

Figure 20. PV output voltage, current and power results

Figure 16 displays the power output results for the PV system and boost converter, confirming the consistent superiority of the FSSO algorithm over the GWO and PSO algorithms. It is worth noting that the FSSO algorithm outperforms the other algorithms in terms of efficiency and power output. The FSSO algorithm efficiently tracks the maximum power point, resulting in an output power amplitude of up to 783.4 W, or an efficiency of 99.42%. In contrast, the PSO and GWO algorithms produce 510.9 W (98.59%) and 399.3 W (92.36%) respectively. When evaluating the performance of the FSSO algorithm in comparison to the GWO and PSO algorithms, it was found that the FSSO algorithm was more efficient. Specifically, it outperformed the PSO algorithm by 34.78% and the GWO algorithm by 49.02%. The power curves generated by the Boost converter were analysed to evaluate the impact of control by various algorithms in a scenario where the photovoltaic (PV) system is connected to a battery. The FSSO algorithm was found to be consistently superior, characterised by fewer oscillations than the In algorithm. The influence of the boost converter output power on the system's DC bus voltages is shown in Figure 17. The relevance of the FSSO algorithm in optimizing energy production is highlighted by these observations on GWO and PSO algorithms. Figure 17 presents the results of the PV system voltage stability when controlled by the FSSO algorithm. The voltages emitted by the PV system and the DC bus remain stable. However, when controlled by the GWO and PSO algorithms, fluctuations occur, reducing the system's performance. This observation confirms the continued effectiveness of the FSSO algorithm. It demonstrates the algorithm's ability to optimize the output power of the Boost converter, as shown in Figure 16. The converter adjusts the DC bus voltage to maximize the power produced by the solar panels by following the maximum power point (MPPT). Additionally, the Boost converter current in the PV system, controlled by the FSSO algorithm, demonstrates remarkable stability, ensuring a more significant optimization of the maximum power point compared to PV systems controlled by other algorithms. These results once again highlight the importance of the FSSO algorithm in optimizing PV system performance and stability. Figure 18 presents a clear representation of the voltage and current variations of the inverter. It is evident that the use of the FSSO algorithm results in greater stability in voltage and current adjustment compared to the GWO and PSO algorithms. This observation is due to the FSSO algorithm's increased efficiency in optimizing the maximum power point, which exceeds the capabilities of the GWO and PSO algorithms. The results emphasize the importance of using the FSSO algorithm to optimize energy production in this specific context. In a photovoltaic system with battery storage, current and voltage are essential for battery operation and system integration. Figure 19 displays the current and voltage results for the storage battery. The findings indicate that irrespective of the algorithm employed to enhance energy generation in the photovoltaic system, the current, which represents the amount of electricity flowing at any given time, remains constant. Furthermore, the battery retains a positive state of charge, as indicated by the positive current. This study presents PV system configurations controlled by the FSSO, GWO, or PSO algorithm. The battery voltage, which determines the amount of stored energy available for use, remains constant in each configuration. The results

demonstrate the effectiveness of each algorithm in optimizing the energy production of the PV system with storage.

4.3 Electric vehicle powered by a photovoltaic battery

The idea of an electric vehicle powered by a photovoltaic battery is intriguing and has led to research and experimentation in sustainable transportation. In this study, we compared the performance of the FSSO, GWO, and PSO algorithms to optimize the vehicle's energy efficiency and make the most of intermittent solar energy. The goal is to offer a more sustainable driving experience. However, achieving this goal requires accurate modeling of system components, precise data collection, and sophisticated algorithms capable of making real-time decisions based on multiple variables. The results obtained in this work are illustrated in Figure 20, Figure 21, and Figure 22. The FSSO algorithm maximizes current while minimizing voltage to achieve optimum power, which is suitable for a parallel string configuration of modules. On the other hand, GWO and PSO algorithms maximize voltage while minimizing current for optimum power, which is adapted to a series of modules' connections. The results indicate that there are power dips between 5 and 10 seconds with FSSO and GWO, while PSO has no dips. The dips in the photovoltaic power curve observed with the FSSO and GWO algorithms could be due to local sub-optimisation. These algorithms may become stuck in solutions that seem optimal at a specific location in the search space but do not represent the global optimum, resulting in a temporary drop in power output. Throughout the period of energy production for an electric vehicle powered by a photovoltaic battery, the PSO technique outperforms the FSSO and GWO algorithms in terms of power output. Figure 21 below illustrates the current and voltage curves of the vehicle's photovoltaic battery. The battery voltage is the electromotive force necessary to power the vehicle's electrical system. The FSSO algorithm produced a maximum value of 51.55 V, slightly higher than the 50.85 V obtained with the GWO and PSO algorithms.

It is worth noting that the voltage delivered by the DC bus varies compared to that of the battery. The reason for this difference is the adjustments made to the battery voltage using devices like the Boost converter to meet the specific requirements of the electric motor and other vehicle components. Whenever the FSSO, GWO or PSO algorithms are employed, a shared characteristic is the substantial energy storage in the battery, which can reach up to 4429 A. This stored current is crucial for the operation of the electric vehicle powered by the photovoltaic battery, as it represents the flow of electrical energy generated by the solar panels and stored in the battery to power the vehicle's engine.

Figure 22 below illustrates the speed, torque, and current of the motor in an electric vehicle powered by a photovoltaic battery. The speed of the motor depends on various factors, including the capacity of the solar panels, energy management, motor efficiency, and vehicle mass.

The results indicate variations in maximum speed between 0 and 5 seconds, depending on the algorithms used. The FSSO algorithm yields a maximum speed of 46.06 rpm, which slightly increases to 46.52 rpm with the PSO algorithm but decreases to 42.08 rpm with the GWO algorithm. Maximizing the output power of the solar photovoltaic panel could increase the energy available to power the electric motor, positively influencing vehicle speed. Between 5 and 10 seconds, the FSSO and GWO algorithms show a decrease in speed, while the PSO algorithm maintains a constant speed. This variation can be attributed to sub-optimisation when adjusting the solar panel's power output, which affects the vehicle's speed. Between 10 and 15 seconds, the speed returns to its initial position. Similar observations were made for torque and motor current. The importance of torque is crucial as it represents the rotational force generated by the motor. Optimizing torque increases the rotation of the drive shaft or wheel, thereby improving traction capacity and overall performance. In conclusion, the PSO algorithm demonstrates the best performance in terms of motor current.

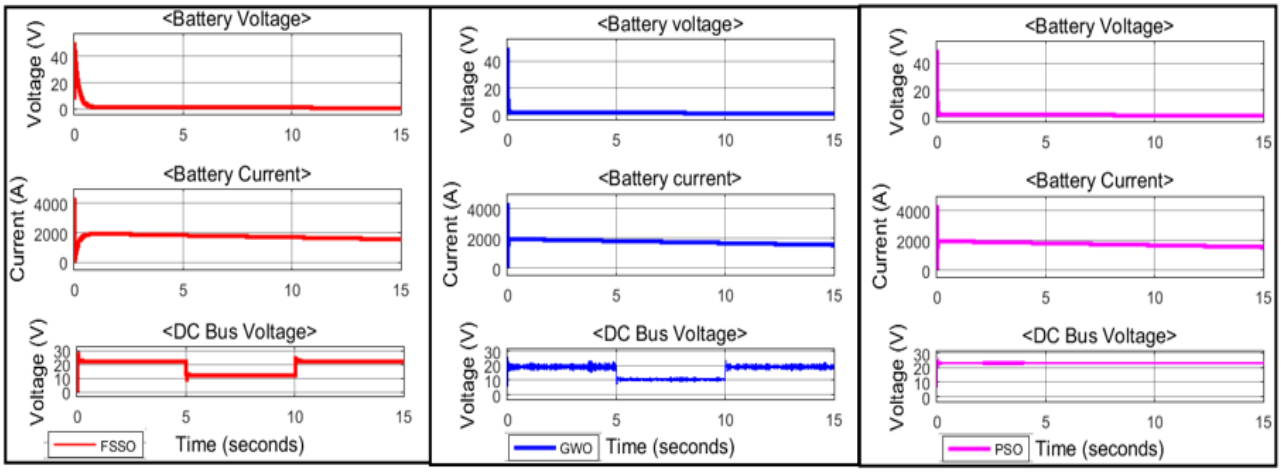

Figure 21. Battery current and voltage results

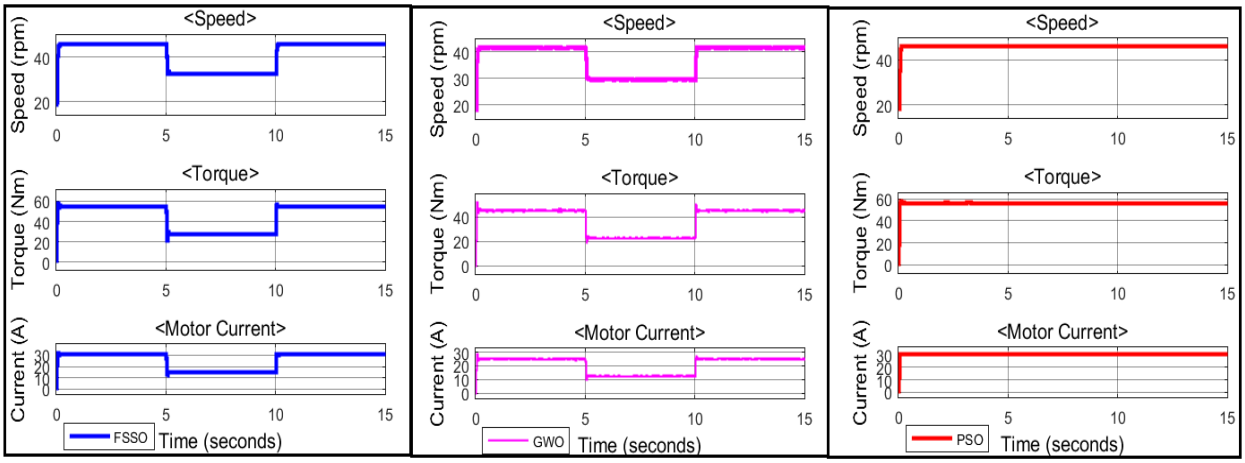

Figure 22. Motor speed, torque and current results

5. Conclusion

Solar energy is a promising solution for meeting the world's energy needs. However, due to its intermittent nature, it requires control to achieve optimal energy production. The FSSO algorithm is an effective method for tracking the point of maximum power. This study compares the FSSO algorithm with other algorithms such as GWO and PSO, demonstrating its superior efficiency of over 99%. The results demonstrate a significant improvement in the convergence time of the FSSO algorithm, reducing it by 16 to over 60% compared to other methods studied. This reduction minimizes more than 80% of random oscillations, contributing to greater stability in tracking the maximum power point. The application of FSSO to Modified ODD-EVEN (MOE), Modified Symmetrical Array (MSA), and Total-Cross-Tied (TCT) configurations showed superior performance in reducing power losses due to partial shading. The FSSO algorithm demonstrated significant advantages with the integration of a bidirectional DC-DC converter connecting the photovoltaic system to a battery, resulting in gains of over 34.78% compared to PSO and 49.02% compared to GWO. Even in the context of an electric vehicle powered by a photovoltaic battery, FSSO remains a promising option, despite slightly lower performance than PSO. The FSSO algorithm is a robust solution for improving photovoltaic energy production in the presence of partial shading. It offers faster maximum power point tracking, reduces computational load, minimizes energy production losses, and increases overall efficiency. These promising results suggest that the FSSO-based approach could be a significant advance in the field of photovoltaic system optimization.

Acknowledgment

The LMSM laboratory at the Institut Nationale Polytechnique, Félix HOUPHOUËT-BOIGNY (Cote d'Ivoire) and the LE3PI laboratory at the Ecole Supérieure Polytechnique (Senegal) staff are acknowledged for providing the necessary equipment.

Ethical issue

The authors are aware of and comply with best practices in publication ethics, specifically concerning authorship (avoidance of guest authorship), dual submission, manipulation of figures, competing interests, and compliance with policies on research ethics. The authors adhere to publication requirements that the submitted work is original and has not been published elsewhere in any language.

Data availability statement

The manuscript contains all the data. However, more data will be available upon request from the authors.

Conflict of interest

The authors declare no potential conflict of interest.

References

[1] N. Rakesh and T. V. Madhavaram, "Performance enhancement of partially shaded solar PV array using novel shade dispersion technique," Front. Energy, vol. 10, no. 2, pp. 227–239, 2016.

[2] S. Pareek, N. Chaturvedi, and R. Dahiya, "Optimal interconnections to address partial shading losses in solar photovoltaic arrays," Sol. Energy, vol. 155, pp. 537–551, 2017.

[3] V. M. R. Tatabhatla, A. Agarwal, and T. Kanumuri, "Enhanced performance metrics under shading conditions through experimental investigations," IET Renew. Power Gener, vol. 14, no. 14, pp. 2592–2603, 2020.

[4] M. Etarhouni, B. Chong, and L. Zhang, "A combined scheme for maximising the output power of a Photovoltaic array under partial shading conditions," Sustain. Energy Technol. Assessments, vol. 50, no. March, 2022.

[5] A. M. Ajmal, T. Sudhakar Babu, V. K. Ramachandaramurthy, D. Yousri, and J. B. Ekanayake, "Static and dynamic reconfiguration approaches for mitigation of partial shading influence in photovoltaic arrays," Sustain. Energy Technol. Assessments, vol. 40, 2020.

[6] S. Sugumar, D. Prince Winston, and M. Pravin, "A novel on-time partial shading detection technique for electrical reconfiguration in solar PV system," Sol. Energy, vol. 225, no. September, pp. 1009–1025, 2021.

[7] S. Rezazadeh, A. Moradzadeh, S. M. Hashemzadeh, K. Pourhossein, B. Mohammadi-Ivatloo, and S. H. Hosseini, "A novel prime numbers-based PV array

reconfiguration solution to produce maximum energy under partial shade conditions," Sustain. Energy Technol. Assessments, vol. 47, no. July, p. 101498, 2021.

[8] M. Zeeshan, N. U. Islam, F. Faizullah, I. U. Khalil, and J. Park, "A Novel Row Index Mathematical Procedure for the Mitigation of PV Output Power Losses during Partial Shading Conditions," Symmetry (Basel), vol. 15, no. 3, 2023.

[9] N. Djilali and N. Djilali, "PV array power output maximization under partial shading using new shifted PV array arrangements," Appl. Energy, vol. 187, pp. 326–337, 2017.

[10] K. S. Faldu and P. S. Kulkarni, "Maximization of the Output Power from Photovoltaic Array under Partial Shading Conditions," 2020 IEEE Int. Students' Conf. Electr. Electron. Comput. Sci. SCEECS 2020, 2020.

[11] A. S. Yadav, R. K. Pachauri, Y. K. Chauhan, S. Choudhury, and R. Singh, "Performance enhancement of partially shaded PV array using novel shade dispersion effect on magic-square puzzle configuration," Sol. Energy, vol. 144, pp. 780–797, 2017.

[12] B. Dhanalakshmi and N. Rajasekar, "A novel Competence Square based PV array reconfiguration technique for solar PV maximum power extraction," Energy Convers. Manag, vol. 174, no. August, pp. 897–912, 2018.

[13] P. R. Satpathy, A. Sarangi, S. Jena, B. Jena, and R. Sharma, "Topology alteration for output power maximization in PV arrays under partial shading," Int. Conf. Technol. Smart City Energy Secur. Power Smart Solut. Smart Cities, ICSESP 2018 - Proc., vol. 2018-Janua, no. March, pp. 1–6, 2018.

[14] S. N. Deshkar, S. B. Dhale, J. S. Mukherjee, T. S. Babu, and N. Rajasekar, "Solar PV array reconfiguration under partial shading conditions for maximum power extraction using genetic algorithm," Renew. Sustain. Energy Rev., vol. 43, no. 2015, pp. 102–110, 2015.

[15] A. Harrag and S. Messalti, "Adaptive GA-based reconfiguration of photovoltaic array combating partial shading conditions," Neural Comput. Appl., vol. 30, no. 4, pp. 1145–1170, 2018.

[16] A. N. M. Mohammad, M. A. M. Radzi, N. Azis, S. Shafie, and M. A. A. M. Zainuri, "A novel hybrid approach for maximizing the extracted photovoltaic power under complex partial shading conditions," Sustain., vol. 12, no. 14, pp. 1–24, 2020.

[17] D. Prince Winston et al., "Parallel power extraction technique for maximizing the output of solar PV array," Sol. Energy, vol. 213, no. January, pp. 102–117, 2021.

[18] R. K. Pachauri et al., "Impact of partial shading on various PV array configurations and different modeling approaches: A comprehensive review," IEEE Access, vol. 8, pp. 181375–181403, 2020.

[19] N. Kacimi, A. Idir, S. Grouni, and M. S. Boucherit, "a New Combined Method for Tracking the Global Maximum Power Point of Photovoltaic Systems," Rev. Roum. des Sci. Tech. Ser. Electrotech. Energ., vol. 67, no. 3, pp. 349–354, 2022.

[20] Y. Zhan, C. Wei, J. Zhao, Y. Qiang, W. Wu, and Z. Hao, "Adaptive mutation quantum-inspired squirrel search algorithm for global optimization problems," Alexandria Eng. J., vol. 61, no. 9, pp. 7441–7476, 2022.

[21] Y. Wang and T. Du, "An improved squirrel search algorithm for global function optimization," Algorithms, vol. 12, no. 4, 2019.

[22] G. Azizyan, F. Miarnaeimi, M. Rashki, and N. Shabakhty, "Flying Squirrel Optimizer (FSO): A novel SI-based optimization algorithm for engineering problems," Iran. J. Optim., vol. 11, no. 2, pp. 177–205, 2019.

[23] D. Kumar et al., "A Novel Hybrid MPPT Approach for Solar PV Systems Using Particle-Swarm-Optimization-Trained Machine Learning and Flying Squirrel Search Optimization," Sustain. 2023, Vol. 15, Page 5575, vol. 15, no. 6, p. 5575, Mar. 2023.

[24] I. Grgić, M. Bašić, and D. Vukadinović, "Optimization of electricity production in a grid-tied solar power system with a three-phase quasi-Z-source inverter," J. Clean. Prod., vol. 221, pp. 656–666, 2019.

[25] D. Yousri, T. S. Babu, E. Beshr, M. B. Eteiba, and D. Allam, "A Robust Strategy Based on Marine Predators Algorithm for Large Scale Photovoltaic Array Reconfiguration to Mitigate the Partial Shading Effect on the Performance of PV System," IEEE Access, vol. 8, pp. 112407–112426, 2020.

[26] N. Rajeswari and S. Venkatanarayanan, "An Efficient Honey Badger Optimization Based Solar MPPT Under Partial Shading Conditions," Intell. Autom. Soft Comput., vol. 35, no. 2, pp. 1311–1322, 2023

[27] A. M. Humada, M. Hojabri, S. Mekhilef, and H. M. Hamada, "Solar cell parameters extraction based on single and double-diode models: A review," Renew. Sustain. Energy Rev., vol. 56, no. January 2020, pp. 494–509, 2016.

[28] K. Ishaque, Z. Salam, H. Taheri, and Syafaruddin, "Modeling and simulation of photovoltaic (PV) system during partial shading based on a two-diode model," Simul. Model. Pract. Theory, vol. 19, no. 7, pp. 1613–1626, 2011.

[29] M. H. Zafar, N. M. Khan, A. F. Mirza, and M. Mansoor, "Bio-inspired optimization algorithms based maximum power point tracking technique for photovoltaic systems under partial shading and complex partial shading conditions," J. Clean. Prod., vol. 309, no. May, p. 127279, 2021.

[30] P. Shaw, "Modelling and analysis of an analogue MPPT-based PV battery charging system utilising DC-DC boost converter," IET Renew. Power Gener., vol. 13, no. 11, pp. 1958–1967, Aug. 2019.

[31] M. Mansoor, A. F. Mirza, and Q. Ling, "Harris hawk optimization-based MPPT control for PV systems under partial shading conditions," J. Clean. Prod., vol. 274, p. 122857, 2020.

[32] T. G. Ragnagnéwendé, "Maximisation du transfert de l ' énergie d ' un champ photovoltaïque tenant compte du phénomène d ' ombrage partiel : connexion réseau électrique par," 2019.

[33] O. Bingöl and B. Özkaya, "Analysis and comparison of different PV array configurations under partial shading conditions," Sol. Energy, vol. 160, no. November 2017, pp. 336–343, 2018.

[34] A. S. Yadav, R. K. Pachauri, and Y. K. Chauhan, "Comprehensive investigation of PV arrays with puzzle shade dispersion for improved performance," Sol. Energy, vol. 129, pp. 256–285, 2016.
[35] M. S. S. Nihanth, J. P. Ram, D. S. Pillai, A. M. Y. M. Ghias, A. Garg, and N. Rajasekar, "Enhanced power production in PV arrays using a new skyscraper puzzle based one-time reconfiguration procedure under partial shade conditions (PSCs)," Sol. Energy, vol. 194, no. October, pp. 209–224, 2019.
[36] G. Meerimatha and B. L. Rao, "Novel reconfiguration approach to reduce line losses of the photovoltaic array under various shading conditions," Energy, vol. 196, p. 117120, 2020.
[37] D. Fares, M. Fathi, I. Shams, and S. Mekhilef, "A novel global MPPT technique based on squirrel search algorithm for PV module under partial shading conditions," Energy Convers. Manag., vol. 230, no. December 2020, p. 113773, 2021.
[38] N. Singh, K. K. Gupta, S. K. Jain, N. K. Dewangan, and P. Bhatnagar, "A Flying Squirrel Search Optimization for MPPT under Partial Shaded Photovoltaic System," IEEE J. Emerg. Sel. Top. Power Electron, vol. 9, no. 4, pp. 4963–4978, 2021.
[39] P. Verma et al., "Meta-heuristic optimization techniques used for maximum power point tracking in solar pv system," Electron., vol. 10, no. 19, pp. 1–57, 2021.
[40] J. Ahmed and Z. Salam, "A Maximum Power Point Tracking (MPPT) for PV system using Cuckoo Search with partial shading capability," Appl. Energy, vol. 119, pp. 118–130, 2014.
[41] Y. Xiaobing, Y. Xianrui, and C. Hong, "An improved gravitational search algorithm for global optimization," J. Intell. Fuzzy Syst., vol. 37, no. 4, pp. 5039–5047, 2019.
[42] M. Jain, V. Singh, and A. Rani, "A novel nature-inspired algorithm for optimization: Squirrel search algorithm," Swarm Evol. Comput., vol. 44, no. November 2017, pp. 148–175, 2019.
[43] D. Yousri, T. S. Babu, E. Beshr, M. B. Eteiba, and D. Allam, "A Robust Strategy Based on Marine Predators Algorithm for Large Scale Photovoltaic Array Reconfiguration to Mitigate the Partial Shading Effect on the Performance of PV System," IEEE Access, vol. 8, pp. 112407–112426, 2020.
[44] B. Qi and J. Wang, "Fill factor in organic solar cells," Phys. Chem. Chem. Phys., vol. 15, no. 23, pp. 8972–8982, 2013.
[45] BLOM, Youri, VOGT, Malte Ruben, RUIZ TOBON, Carlos M., et al. Energy Loss Analysis of Two-Terminal Tandem PV Systems under Realistic Operating Conditions—Revealing the Importance of Fill Factor Gains. Solar RRL, 2023, p. 2200579.
[46] M. Dhimish, V. Holmes, B. Mehrdadi, M. Dales, B. Chong, and L. Zhang, "Seven indicators variations for multiple PV array configurations under partial shading and faulty PV conditions" Renewable Energy, 2017 (pages 438-460) https://doi.org/10.1016/j.renene.2017.06.014